Medical Engineering and Physics 130 (2024) 104213

Contents lists available at ScienceDirect

Medical Engineering and Physics

journal homepage: www.elsevier.com/locate/medengphy

Paper

An efficient channel recurrent Criss-cross attention network for epileptic seizure prediction

Lei Zhu [a,*], Wentao Wang [a], Aiai Huang [a], Nanjiao Ying [a], Ping Xu [a], Jianhai Zhang [b,c]

[a] School of Automation, Hangzhou Dianzi University, Hangzhou 310000, PR China
[b] School of Computer Science, Hangzhou Dianzi University, Hangzhou 310000, PR China
[c] Key Laboratory of Brain Machine Collaborative Intelligence of Zhejiang Province, Hangzhou 310018, PR China

ARTICLE INFO

Keywords:
EEG
Epilepsy prediction
Classification algorithm
Spectrogram
Short-time fourier transform
Attention

ABSTRACT

Epilepsy is a chronic disease caused by repeated abnormal discharge of neurons in the brain. Accurately predicting the onset of epilepsy can effectively improve the quality of life for patients with the condition. While there are many methods for detecting epilepsy, EEG is currently considered one of the most effective analytical tools due to the abundant information it provides about brain activity. The aim of this study is to explore potential time-frequency and channel features from multi-channel epileptic EEG signals and to develop a patient-specific seizure prediction network. In this paper, an epilepsy EEG signal classification algorithm called Channel Recurrent Criss-cross Attention Network (CRCANet) is proposed. Firstly, the spectrograms processed by the short-time fourier transform is input into a Convolutional Neural Network (CNN). Then, the spectrogram feature map obtained in the previous step is input into the channel attention module to establish correlations between channels. Subsequently, the feature diagram containing channel attention characteristics is input into the recurrent criss-cross attention module to enhance the information content of each pixel. Finally, two fully connected layers are used for classification. We validated the method on 13 patients in the public CHB-MIT scalp EEG dataset, achieving an average accuracy of 93.8 %, sensitivity of 94.3 %, and specificity of 93.5 %. The experimental results indicate that CRCANet can effectively capture the time-frequency and channel characteristics of EEG signals while improving training efficiency.

1. Introduction

Epilepsy is a chronic neurological disorder caused by recurrent abnormal discharges of neurons in the brain, and it is classified as a noninfectious disease. According to statistics, there are >50 million epilepsy patients in the world [1], with an average incidence of 23–190 per 100,000 people [2]. Repeated seizures can have a continuous negative impact on the patient's mental health and may even endanger their lives. Therefore, the diagnosis and treatment of epilepsy are of vital clinical significance.

Electroencephalogram (EEG) has been used for many years to analyze and record epilepsy, and is regarded as one of the most important diagnostic tools for the condition [3,4]. Scalp electroencephalogram (sEEG) collects microvolt electrical signals generated by synchronous neuronal activity in the brain through electrodes placed at specific locations on the scalp. Due to easy access and low cost, sEEG has been the most widely used non-invasive EEG detection with a history of >70 years [5-7].

According to previous research, the electrical activity of the brain in patients with epilepsy is generally classified into four distinct periods [8,9]. As illustrated in Fig. 1, these periods include interictal period, preictal period, ictal period and postictal period. Additionally, SPH (Seizure Prediction Horizon) represents the interval between the issuance of a seizure warning and the onset of the seizure. The SPH should be long enough to allow patients sufficient time to take measures for intervention and treatment after receiving the warning. Studies have shown that the transition from a normal state to an epileptic state is not sudden [10]. Instead, it often involves a transitional period known as the preictal period. The primary task of this study is to accurately identify preictal signals in epileptic EEG data. While previous research on epilepsy has focused on epileptic seizure detection, which involves the classification and recognition of ictal signals. Successfully detecting epileptic signals in massive EEG signals can greatly reduce the time cost of EEG labeling for doctors and researchers, which has important

* Corresponding author.
E-mail address: zhulei@hdu.edu.cn (L. Zhu).

https://doi.org/10.1016/j.medengphy.2024.104213
Received 1 August 2023; Received in revised form 8 July 2024; Accepted 31 July 2024
Available online 8 August 2024

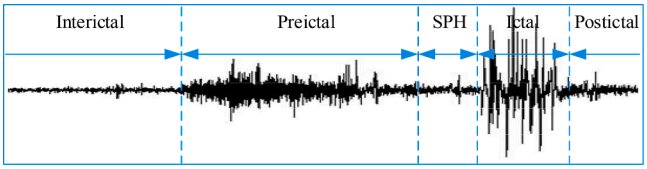

Fig. 1. Example of an EEG during different seizure periods.

research significance. However, accurately identifying preictal signals seems to be more meaningful, as it enables patients to receive timely treatment and gives doctors more time to prepare for rescue efforts.

Generally speaking, the seizure prediction process is depicted in Fig. 2. It involves EEG acquisition, signal preprocessing, feature extraction and classification prediction. Due to the nonlinear, non-stationary, and weak nature of raw EEG signals, data preprocessing operations are generally performed before feature extraction [11]. Common preprocessing methods currently include Wavelet Transform (WT), Short-Time Fourier Transform (STFT), Empirical Mode Decomposition (EMD), and others. Hasan Ocak et al. [12] processed raw EEG signals using WT and employed the approximate entropy method to measure the complexity of sub-band signals. Experimental results revealed a 23 % improvement in prediction accuracy after preprocessing compared to before preprocessing. Islam et al. [13] selected the stationary WT to eliminate artifacts from single-channel EEG data, thus lowering false alarm rates in seizure detection and improving the accuracy and reliability of the process. Truong et al. [14] performed Short-Time Fourier Transform on epileptic EEG signals to generate spectrograms, which were subsequently utilized as inputs for the feature extraction stage. This significantly enhanced the performance of seizure prediction. Parhi et al. [15] employed bipolar and time difference methods for preprocessing EEG signals to mitigate electrode noise and artifacts common to all electrodes. This approach achieves the highest classification accuracy in under 0.028 s.

After preprocessing the data, feature extraction can be performed on it. Feature extraction plays a pivotal role in seizure prediction. Commonly used methods for feature extraction include power spectral density, wavelet energy, permutation entropy, maximum Lyapunov exponent, phase locking value, Hurst exponent, Hjorth parameters, etc. [16-19] As an important branch of machine learning, deep learning has attracted much attention because of its powerful characterization ability and excellent performance, and has excellent performance in medical image and biological signal processing [20]. Unlike traditional methods of feature extraction and classification prediction, deep learning typically integrates these two processes, forming a complete end-to-end learning framework. Common deep learning models include Convolutional Neural Networks (CNN), Recurrent Neural Networks (RNN), Long Short-term Memory networks (LSTM), and Transformers. Currently, most epilepsy prediction models are also built upon enhancements to these aforementioned deep learning models. Daoud et al. [21] input raw epileptic EEG signals into a network consisting of a Deep Convolutional Autoencoder (DCAE) and a Bidirectional Long Short-term Memory network (Bi-LSTM), achieving significantly high prediction accuracy. Abdelhameed et al. [22] employed a two-dimensional Convolutional Variational Autoencoder (CVAE), trained it in a supervised manner, and successfully achieved automatic feature learning and classification of epileptic signals within a prediction window lasting up to one hour. Zhang et al. [23] computed the Pearson correlation coefficient of EEG signals and inputted the resulting correlation matrix into a three-layer CNN, achieving an accuracy of 89.98 %. Hu et al. [24] input the Mean Amplitude Spectrum (MAS) into a CNN to extract features and classified them using Support Vector Machine (SVM), achieving a classification accuracy of 86.25 %. Cao et al. [25] stacked multiple CNNs and fused the outputs of these networks with weighted fusion. This architecture effectively utilized MAS as input data for the neural network. Experimental results demonstrate that this design achieved high classification performance. Usman et al. [26] input the preprocessed spectrograms into a network that combined SVM, CNN and LSTM, and achieved 96.28 % sensitivity and 95.65 % specificity. Liu et al. [27]. input the spectrograms into a hybrid bilinear model and achieved F1-score of 97.4 % and 97.2 % from TUH dataset and EPILEPSIAE dataset, respectively. The attention mechanism can focus on the more critical information among many information, so as to improve the efficiency and accuracy of model training. Yang et al. [28] combined the Residual Network (ResNet) and the dual self-attention mechanism to get a dual self-attention residual network (RDANet). The network could extract positional attention and channel attention from spectral feature maps and was tested on 13 patients in the CHB-MIT dataset. It achieved the sensitivity of 89.33 %, the specificity of 93.02 % and the accuracy of 92.07 %.

EEG contains rich time-frequency and channel information, which is invaluable for epilepsy research. To leverage this information effectively, this paper proposes an innovative Channel Recurrent Criss-cross Attention Network (CRCANet) based on EEG. The core of this network architecture consists of two main modules: the channel attention module and the recurrent criss-cross attention module. The channel attention module explores potential dependencies among different EEG channels, establishing correlations among them. Additionally, the recurrent criss-cross attention module aims to enhance the global information content of each pixel in the feature map, improving its pixel-level representation capability. The synergistic effect of these two modules greatly enhances the representational power of the original feature map, enabling CRCANet to achieve outstanding performance in seizure prediction tasks. We verified our proposed method on the CHB-MIT dataset and compared it with other three typical models.

2. Materials and methods

2.1. Dataset

In this study, we utilized the CHB-MIT sEEG dataset [29,30] for our research. It comprises EEG signals recorded at Boston Children's Hospital, consisting of 23 records from 22 subjects. All EEGs were recorded using bipolar montage technology from the International 10–20 system at a sampling rate of 256 Hz [31].

The research indicates that within the 50 min preceding an epileptic seizure, the accumulated energy in the brain's electrical signals gradually increases, while the brain's electrical signals tend to stabilize in the 5 to 30 min following the end of the seizure [32,33]. Therefore, this study defines the preictal period as the 35-minute interval preceding an epileptic seizure, and the interictal period as the time range from 30 min after the seizure to 30 min before the onset of the next seizure [34]. To implement effective preventive measures, it's crucial to allocate a short time window before the seizure occurs as an intervention period (SPH). In this study, the SPH was set to 5 min [9,14,21,35], and data within this

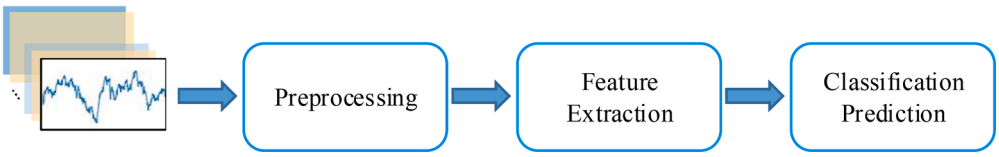

Fig. 2. Epileptic seizure prediction process.

timeframe were excluded from the original dataset. According to the studies of Truong et al. [14], for patients who had seizures on average every two hours, performing the prediction task was not very important. Therefore, we only considered patients who had fewer than 10 seizures per day. Consequently, we selected 27.7 h of preictal data from 64 recordings involving 13 epileptic patients in the CHB-MIT dataset for analysis. Our selection criteria included at least 3 major seizures and a 3-hour interictal period record, which ensured that we had sufficient data samples for analysis, as shown in the Table 1.

2.2. Preprocessing

Given that epileptic seizures are rare events, the amount of preictal data in the dataset is usually much smaller compared to the interictal data. Consequently, a classifier trained on such imbalanced data would likely exhibit bias towards the larger class [36]. To address the imbalance between preictal and interictal data, we referenced the method proposed by Yang et al. [28], which involves using a sliding window with overlapping and truncating data during the acquisition of prediction data. The length of the preictal period is denoted as$P$, the length of the interictal period as$I$, the length of the sliding window as$W$, and the data length ratio between the preictal period and the interictal period as$R$(Formula (1)). The data volume$p$of the preictal period and$i$of the interictal period are calculated using Formula (2) and 3, respectively.

$$R = \frac{P}{I} \tag{1}$$

$$p = \frac{P - W}{W \times R} + 1 \tag{2}$$

$$i = \frac{I - W}{W} + 1 \tag{3}$$

To ensure the diversity of each preictal sample and prevent adverse effects on model training, we maintained the$R$value within the range of 0.25 to 1.0. Additionally, based on previous research findings[9,28,37], we set the sliding window length$W$to 5 s. With these parameters in place, we obtained the final sample size for each patient, as detailed in Table 2.

Spectrograms, compared to time-domain and frequency-domain signals, contain more abundant time-frequency information and have proven significantly effective in the detection, prediction, and type classification of epilepsy [27,38]. In this study, spectrograms obtained after STFT were used as the input of neural network. Since the EEGs recorded in the CHB-MIT dataset were subject to power frequency interference near 60 Hz, data from the 57–63 Hz and 117–123 Hz frequency bands were removed to eliminate noise [14]. As shown in the Fig. 3, the horizontal axis of the conversion of the original EEG signal into a spectrogram is the frequency axis, while the vertical axis is the time axis. Fig. a and Fig. b correspond to the images before and after filtering, respectively.

Table 1
The number of seizures and available preictal data duration of 13 patients in the CHB-MIT dataset.

Patient id	No. of seizures	Available preictal hours/h
Pt01	7	2.5
Pt02	3	1.5
Pt03	6	2.0
Pt05	5	2.5
Pt09	4	2.0
Pt10	6	3.0
Pt13	5	2.2
Pt14	5	2.4
Pt18	6	2.0
Pt19	3	1.0
Pt20	5	2.1
Pt21	4	2.0
Pt23	5	2.5
total	64	27.7

Table 2
The total number of samples for each patient's preictal and interictal data after balancing the samples using the sliding window algorithm in the CHB-MIT dataset.

Patient id	Sample size	Patient id	Sample size
Pt01	7069	Pt14	4199
Pt02	4376	Pt18	5748
Pt03	4286	Pt19	2874
Pt05	5740	Pt20	5461
Pt09	5784	Pt21	5704
Pt10	11,502	Pt23	5701
Pt13	4376		

2.3. Model

This study proposes an epileptic seizure classification prediction model, named the CRCANet, as shown in Fig. 4. The model consists of a CNN, a channel attention module, and a recurrent criss-cross attention module. The execution flow of the entire model is outlined as follows:

Firstly, input the spectrograms of EEG signals into the network and extract potential time-frequency features using a basic CNN.

Then, the channel attention module is employed to establish correlations among different EEG channels. The main steps are as follows: Firstly, generating a channel attention matrix to describe the spatial relationships between channels. Secondly, performing matrix multiplication between the original matrix and the attention matrix. Thirdly, adding the resulting matrix from the last step to the original matrix to obtain the final feature map with established channel correlations.

Subsequently, the recurrent criss-cross attention module is utilized to enhance the global information content of each pixel in the feature map. The main steps are as follows: Firstly, generating feature map Query (Q), Key (K), and Value (V) matrices, and using the Q and K matrices to generate a criss-cross attention matrix describing the spatial relationships between horizontal and vertical pixels in the feature map (where horizontal pixels represent frequency features of the feature map, and vertical pixels represent time features). Secondly, performing matrix multiplication between the criss-cross attention matrix and the V matrix, where each pixel aggregates information from its criss-cross paths. Thirdly, adding the resulting matrix to the original matrix, thereby enhancing the weight of the original information for each pixel in the feature map. The fourth step entails repeating the previous steps. Given that each pixel in the current feature map already incorporates features from its criss-cross paths, reiterating these steps allows each pixel to further assimilate global information. In this process, the original information's weight is maximized, followed by that of information in the same horizontal and vertical directions, with the weights of other information minimized.

Finally, the feature matrices from the previous stage are added together again, and the final classification prediction is made through two fully connected (FC) layers .

2.3.1. Convolutional neural network

In various fields of biomedical research, CNNs have proven to be effective[39]. This study addresses the complexity of epileptic EEG data by devising a CNN model consisting of four convolutional blocks. These blocks extract features from the input data, capturing underlying patterns and correlations in epileptic EEG signals. The specific network structure is shown in Fig. 5. The input of the network are the spectrograms of EEG, and the initial input dimension is 64×22×9×114. Here, 64 denotes the batch size, 22 indicates the number of channels in the EEG signals, while 9×114 signifies the dimensions of each spectrogram. The hidden layer of CNN comprises four convolutional blocks, with each block followed by a batch normalization layer, a dropout layer, and a

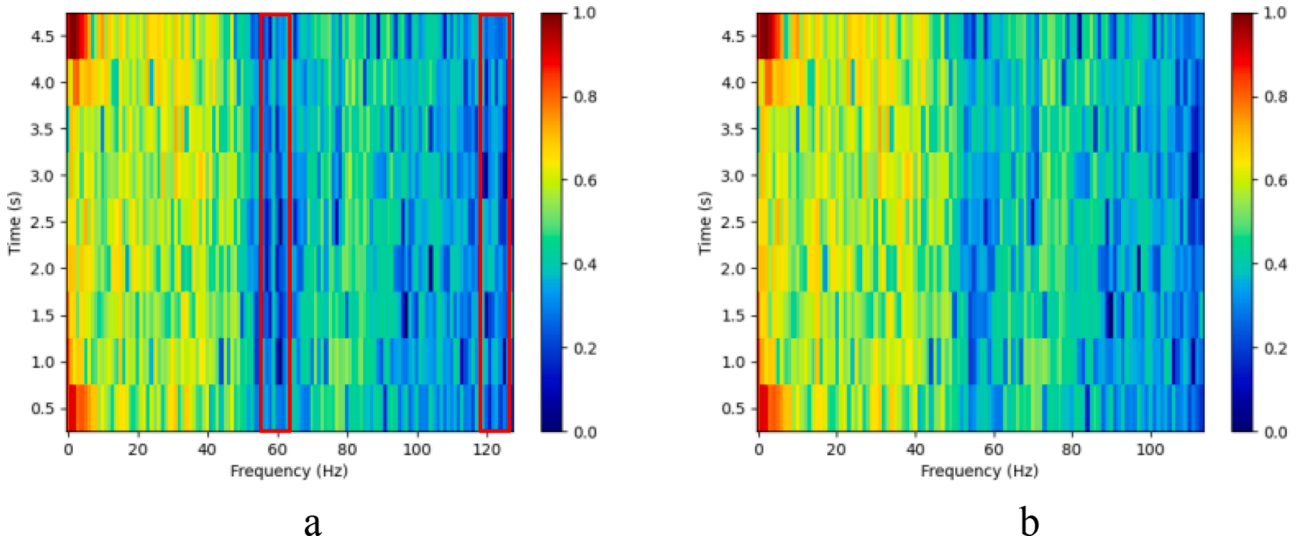

Fig. 3. Comparison before and after filtering (In Fig. a, the red box highlights the EEG signal frequency band contaminated by power line interference, which has been filtered out in Fig. b).

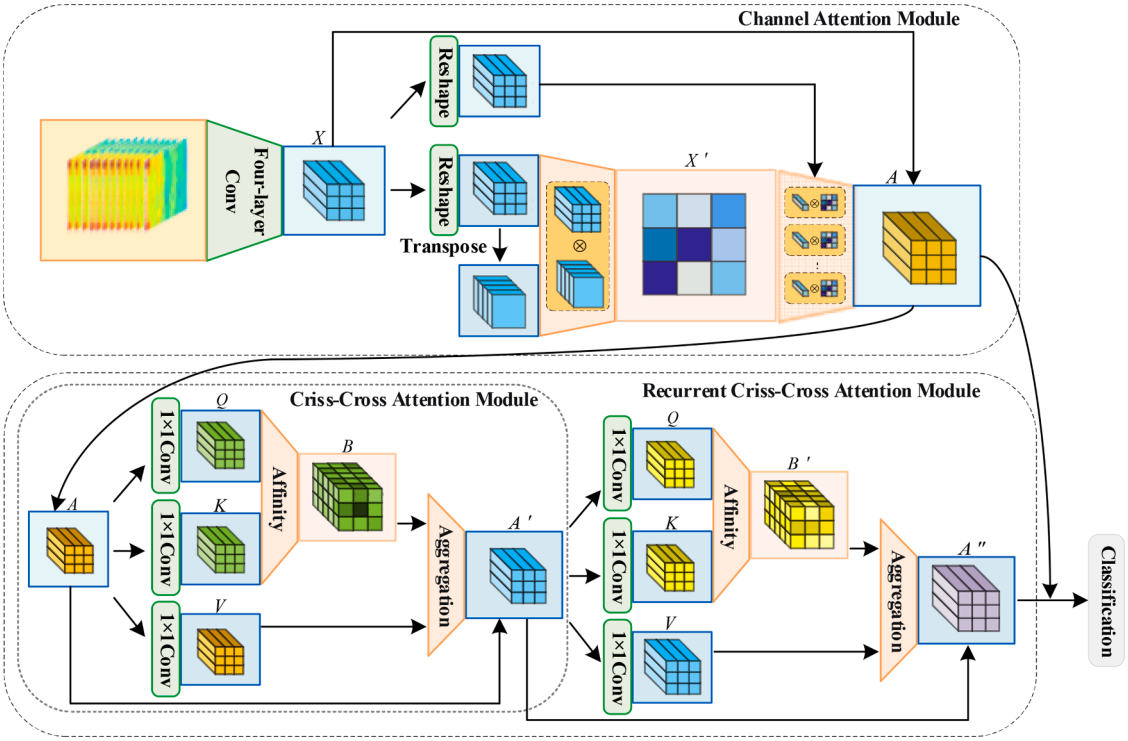

Fig. 4. The structure diagram of CRCANet (The right side of the upper part of the figure is the channel attention module, and the lower half is the recurrent criss-cross attention module composed of two criss-cross attention modules).

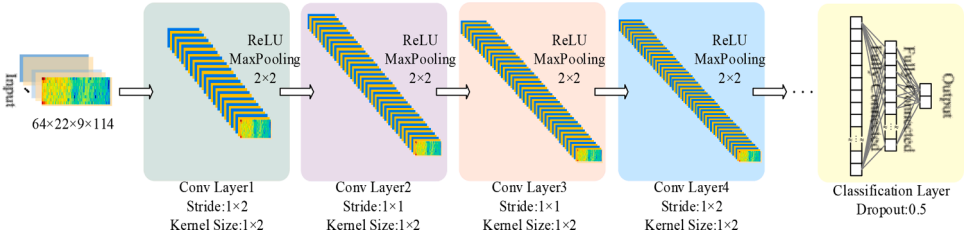

Fig. 5. CNN topology structure.

ReLU activation function. After feature extraction through the four convolutional blocks, the feature maps are enriched by a channel attention module and a recurrent criss-cross attention module. Finally, the final classification result is output through two fully connected layers. Table 3 presents the specific network parameters of CRCANet.

2.3.2. Channel attention module

The channel attention module utilizes the interdependence among channel mappings to establish the correlation between the feature mappings of different channels [40]. Fig. 4 shows the specific structure of the channel attention module. Assuming the original feature map is represented by $X \in \Re^{C\times H\times W}$, we reshape X into $X \in \Re^{C\times N}$, where $N = H \times W$. Then, we perform matrix multiplication between X and its transpose. The resulting matrix is normalized through softmax, obtaining the channel attention matrix $X' \in \Re^{C\times C}$ [28,40]:

$$x'_{ji} = \frac{e^{X_i \cdot X_j}}{\sum_{i=1}^{C} e^{X_i \cdot X_j}} \tag{4}$$

where x'_{ji} represents the result of interaction between channel i and channel j. Then, X' is multiplied with X to obtain the feature matrix (Its dimension is $\Re^{C\times H\times W}$). Next, the result is multiplied by a scaling parameter β (β starts at 0, and it will gradually learn an optimal weight). Finally, adding the corresponding elements of the matrix to the original feature X yields the output $A \in \Re^{C\times H\times W}$ [28,40]:

$$A_j = \beta \sum_{i}^{C} \left(x'_{ji} X_i\right) + X_j \tag{5}$$

2.3.3. Criss-cross attention module

The horizontal and vertical dimensions of the spectrograms respectively carry crucial information about frequency and time. Processed through the criss-cross attention module, each pixel aggregates important information from the same time and frequency, thereby enhancing the representational capacity of each pixel. As shown in the Fig. 4, the feature map $A \in \Re^{C\times H\times W}$ is input into the criss-cross attention module. Initially, three 1×1 convolutions are applied to obtain the Q, K and V matrices, where $\{Q, K\} \in \Re^{C'\times H\times W}$, and C' is the result of dimensionality reduction of C. Next, the Affinity operation is performed on Q and K to obtain the attention diagram $P \in \Re^{(H+W-1)\times(H\times W)}$. As shown in the Fig. 6, for every position m of Q in the space dimension, a vector $Q_m \in \Re^{C'}$ can be got. And feature vectors can be extracted from corresponding rows and columns in K to get a vector set $\Phi_m \in \Re^{(H+W-1)\times C'}$, then the **A**ffinity operation is performed according to Formula (6) [41]:

Table 3
The parameter table of CRCANet structure.

Layer name	Output size	Network structure
Input	64×22×9×114	–
Conv1	64×32×10×29	Kennel size: 1×2, Stride: 1×2, Max pooling: 2×2
Conv2	64×64×6×15	Kennel size: 1×2, Stride: 1×1, Max pooling: 2×2
Conv3	64×128×4×8	Kennel size: 1×2, Stride: 1×1, Max pooling: 2×2
Conv4	64×256×3×3	Kennel size: 1×2, Stride: 1×2, Max pooling: 2×2
Channel attention module	64×256×3×3	–
Recurrent criss-cross attention module	64×256×3×3	–
FC1	64×256	Sigmoid, Dropout: 0.5
FC2	64×2	Dropout: 0.5

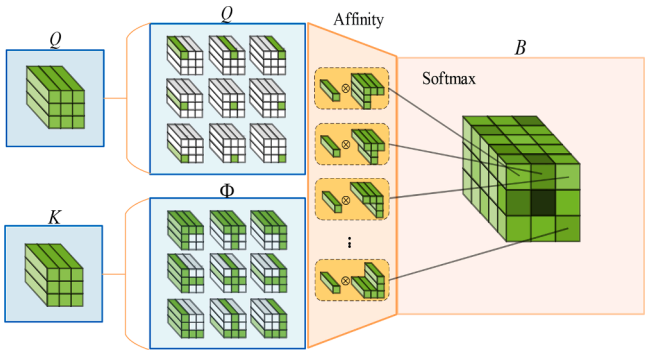

Fig. 6. Affinity operation process diagram.

$$l_{i,m} = Q_m^T \Phi_{i,m} \tag{6}$$

Where $\Phi_{i,m} \in \Re^{C'}$ is the i^{th} element of Φ_m, $l_{i,m} \in L$ expresses the degree of correlation between Q_m and $\Phi_{i,m}$, where $L \in \Re^{(H+W-1)\times(H\times W)}$. After the Affinity operation is performed for Q and K, the result L is normalized through softmax, and the criss-cross attention matrix B is obtained. Then, B needs to do the **A**ggregation operation, as shown in Fig. 7, with $V \in \Re^{C\times H\times W}$. V is used for feature adaptation. $V_m \in \Re^{C}$ is a vector at position m in the spatial dimension of V. $\Psi_m \in \Re^{(H+W-1)\times C}$ is a collection of vectors in the same row and column as V_m. The final feature map is obtained by Formula (7) [41] :

$$A'_m = \sum_{i=0}^{H+W-1} B_{i,m} \Psi_{i,m} + A_m \tag{7}$$

where $B_{i,m}$ is the weight given at position m to the i^{th} vector ($i = [1,2,\ldots,H + W - 1]$). $B_{i,m}$ is a scalar. $A'_m \in \Re^{C}$ is the feature vector at the position m calculated by the criss-cross attention module.

2.3.4. Recurrent criss-cross attention module

A criss-cross attention module allows every pixel in the spectrogram to gather information from its criss-cross paths. However, information from pixels outside this scope cannot be acquired. In order to solve this problem, we stack two criss-cross attention modules. The first module enables each pixel in the feature map to gather information from its corresponding criss-cross paths. Subsequently, the second module replicates the same process, enabling each pixel to acquire global information. As shown in the recurrent criss-cross attention module section in Fig. 4, the feature map A' is input into the other criss-cross attention module. Then a new feature map A'' is obtained. Thus, each pixel in the feature map A'' contains the full time and frequency information of the entire feature map [41].

It is known that the criss-cross attention module can gather information from other pixels along the criss-cross paths of a certain pixel. It is actually a one-to-one mapping relationship. The relation is repre-

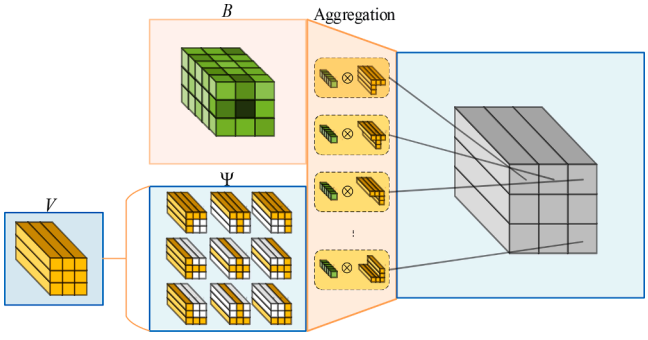

Fig. 7. Aggregation operation process diagram.

sented by f in this paper. Information from pixels not on the criss-cross paths of the pixel is obtained using the method depicted in Fig. 8. Suppose we want to map information from point (b_1, b_2) to point (a_1, a_2), there are two paths. First, the information in (b_1, b_2) is mapped to (b_1, a_2) and (a_1, b_2) in its horizontal and vertical directions. The mapping functions are $f(b_1, b_2, b_1, a_2)$ and $f(b_1, b_2, a_1, b_2)$, respectively. The mapped points (b_1, a_2) and (a_1, b_2) are located vertically and horizontally at (a_1, a_2). Then, the information is again mapped to (a_1, a_2) through mapping function $f(b_1, a_2, a_1, a_2)$ and $f(a_1, b_2, a_1, a_2)$.

Obviously, the recurrent criss-cross attention module can capture global context information, addressing the limitations of a single criss-cross attention module.

3. Results

3.1. Experimental setup and evaluation metrics

In this study, we used the Pytorch deep learning framework and programmed in the Python environment. The version of Pytorch is 1.11.0, the version of Python is 3.8.13, and the version of CUDA is 11.3. The experimental platform is a 64-bit operating system equipped with an Intel ® Core™ i5–11300H @ 3.10 GHz processor. BCEWithLogitsLoss was employed as the loss function, Adam was used as the optimizer, and the model was trained over 200 epochs. The performance of the algorithm was assessed through five-fold cross-validation, with 80 % of the data used for model training and the remaining 20 % for testing. The model's performance was measured using three metrics: Accuracy (Acc), Sensitivity (Sens), and Specificity (Spec). Accuracy reflects the overall proportion of correct predictions, while Sensitivity and Specificity indicate the accuracy of predictions for preictal and interictal data, respectively. The calculation methods for these metrics are as follows:

$$Acc = \frac{TP + TN}{TP + FP + TN + FN} \tag{8}$$

$$Sens = \frac{TP}{TP + FN} \tag{9}$$

$$Spec = \frac{TN}{TN + FP} \tag{10}$$

where TP represents predicting preictal samples as preictal, indicating true positives; TN represents predicting interictal samples as interictal, indicating true negatives; FP represents predicting interictal samples as preictal, indicating false positives; FN represents predicting preictal samples as interictal, indicating false negatives [37].

It is worth noting that our CRCANet topologies is trained and fine-tuned on the CHB-MIT dataset. In order to verify the superiority of our model, we used a set of parameters to compare the experimental models during the experiment. Since RDANet is based on ResNet, we used the parameters mentioned in the work [28]. In addition, we also combined CNN directly with the recurrent criss-cross attention module, CNN directly with the channel attention module, called them RCANet and CANet respectively. By comparing CRCANet, RCANet, and CANet, we can find the effect of different modules on the performance of the model.

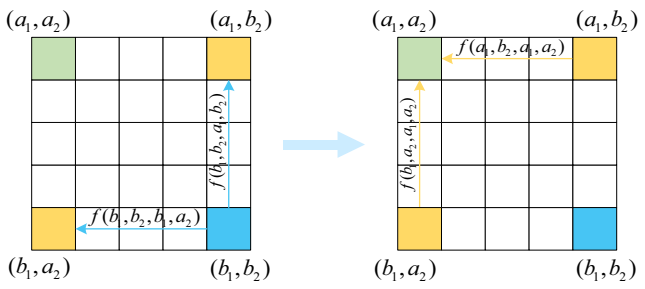

Fig. 8. Information transmission process under the action of the recurrent criss-cross attention.

3.2. Comparative experiments

The test results of CNN, RDANet, CANet, RCANet and CRCANet models on 13 patients from the CHB-MIT dataset are shown in Table 4, Table 5 and Table 6. The experimental results are expressed as the mean ± standard deviation.

Table 4 presents a comparison of the accuracy achieved by five models on 13 patients. For patients Pt09, Pt19, Pt20, and Pt23, using CNN alone achieved good classification results. Although our CRCANet improved their classification accuracy, the improvement was minimal. However, in certain patients, our model showed significant improvements in accuracy. For example, the accuracy of CRCANet was 1.1 % and 1.2 % higher than that of CNN for Pt02 and Pt14, respectively. Both RCANet and CRCANet achieved an accuracy of 87.7 % for Pt05, which was 2.5 % higher than CNN's accuracy. Similarly, for Pt21, the accuracies of RCANet and CRCANet were 79.8 % and 79.9 %, respectively, representing an improvement of 1.5 % and 1.6 % over CNN. CANet also showed some improvement compared to CNN, although it was not substantial. Overall, CRCANet achieved the highest classification accuracy in 10 out of the 13 patients, except for Pt10, Pt19, and Pt23, and its results were very close to those of RDANet, which performed best on these three patients.

Table 5 presents a comparison of the sensitivity of the five models on 13 patients. Similarly, for patients Pt09, Pt19, Pt20, and Pt23, CNN alone achieved good sensitivity indices. All five models achieved a classification sensitivity of >99.0 %, with sensitivities being close to 100 % on Pt09, Pt20, and Pt23. Overall, CRCANet achieved the highest sensitivity in 8 patients, except for Pt05, Pt10, Pt14, Pt21 and Pt23. RCANet and CANet achieved the highest sensitivity in Pt05 and Pt14, respectively. RDANet exhibited the highest sensitivity for Pt10 and Pt21, indicating its superior performance in identifying preictal data for these patients. In summary, CRCANet had the best performance on sensitivity indicators.

Table 6 shows the comparison of the five models' specificity on 13 patients. The specificity of the five models for Pt09, Pt19, Pt20 and Pt23 remained close, all exceeding 99.0 %. CRCANet exhibited the highest specificity in 7 out of 13 patients, while RCANet achieved the highest specificity in 4 patients. Additionally, CANet and CNN demonstrated superior specificity in Pt05 and Pt18, respectively, compared to other models. In general, CRCANet had the best performance on specificity indicators.

The experimental results above demonstrate that the channel attention module in CRCANet effectively establishes connections among

Table 4
Accuracy(%)±std of five models on 13 patients in the CHB-MIT dataset.

Patient ID	CNN	RDANet	Ours		
			CANet	RCANet	CRCANet
Pt01	98.6 ± 0.4	98.1 ± 0.4	98.7 ± 0.5	98.8 ± 0.6	**99.3 ± 0.2**
Pt02	91.4 ± 0.8	91.1 ± 0.9	91.1 ± 0.9	91.7 ± 0.9	**92.5 ± 0.5**
Pt03	98.8 ± 0.3	99.1 ± 0.4	99.2 ± 0.2	99.0 ± 0.6	**99.5 ± 0.3**
Pt05	85.2 ± 0.8	85.9 ± 1.0	86.8 ± 0.7	**87.7 ± 0.3**	**87.7 ± 0.6**
Pt09	**99.9 ± 0.1**	99.8 ± 0.2	**99.9 ± 0.1**	**99.9 ± 0.1**	**99.9 ± 0.1**
Pt10	94.7 ± 0.5	**95.9 ± 0.3**	95.3 ± 0.3	95.4 ± 0.7	95.5 ± 0.5
Pt13	95.0 ± 1.3	94.0 ± 1.2	95.5 ± 0.8	96.0 ± 0.7	**96.1 ± 0.6**
Pt14	72.8 ± 1.9	67.9 ± 1.1	73.1 ± 1.0	73.0 ± 2.3	**74.0 ± 1.4**
Pt18	95.4 ± 0.3	93.9 ± 0.5	95.1 ± 0.8	95.3 ± 0.4	**96.0 ± 0.5**
Pt19	99.0 ± 0.4	**99.4 ± 0.2**	99.2 ± 0.4	99.1 ± 0.2	99.2 ± 0.3
Pt20	99.7 ± 0.1	99.7 ± 0.2	99.8 ± 0.1	**99.9 ± 0.1**	**99.9 ± 0.1**
Pt21	78.3 ± 1.2	76.9 ± 0.6	79.0 ± 0.8	79.8 ± 1.1	**79.9 ± 0.8**
Pt23	99.4 ± 0.3	**99.8 ± 0.1**	99.6 ± 0.2	99.5 ± 0.2	99.7 ± 0.1
Average	92.9	92.4	93.3	93.5	**93.8**

Table 5
Sensitivity(%)±std of five models on 13 patients in the CHB-MIT dataset.

Patient ID	CNN	RDANet	Ours		
			CANet	RCANet	CRCANet
Pt01	98.7 ± 0.5	98.6 ± 0.2	98.3 ± 0.9	98.8 ± 0.8	**99.2 ± 0.2**
Pt02	92.1 ± 1.2	91.5 ± 1.0	93.1 ± 0.7	92.5 ± 2.6	**94.1 ± 1.9**
Pt03	99.4 ± 0.2	99.3 ± 0.7	99.0 ± 0.5	99.3 ± 0.8	**99.5 ± 0.6**
Pt05	84.6 ± 2.6	84.5 ± 1.0	85.0 ± 1.8	**87.4 ± 1.7**	87.1 ± 1.7
Pt09	99.9 ± 0.1	99.9 ± 0.2	99.9 ± 0.1	99.9 ± 0.2	**100.0 ± 0.0**
Pt10	95.1 ± 1.0	**97.1 ± 0.4**	95.7 ± 0.8	96.2 ± 1.3	95.4 ± 0.7
Pt13	95.7 ± 1.9	94.0 ± 1.5	95.6 ± 1.4	96.5 ± 1.6	**96.6 ± 0.5**
Pt14	72.7 ± 3.3	68.3 ± 2.3	**75.4 ± 1.9**	74.9 ± 3.4	73.7 ± 3.3
Pt18	95.7 ± 0.8	95.1 ± 1.5	95.8 ± 1.4	96.9 ± 1.1	**97.3 ± 0.4**
Pt19	99.2 ± 0.1	99.2 ± 0.4	99.2 ± 0.4	99.3 ± 0.4	**99.4 ± 0.3**
Pt20	**99.9 ± 0.1**	**99.9 ± 0.2**	**99.9 ± 0.2**	**99.9 ± 0.1**	**99.9 ± 0.1**
Pt21	83.1 ± 3.9	**85.9 ± 5.8**	84.2 ± 3.6	84.1 ± 1.5	84.0 ± 2.1
Pt23	99.6 ± 0.2	**99.9 ± 0.0**	**99.9 ± 0.1**	99.7 ± 0.3	99.8 ± 0.1
Average	93.5	93.3	93.9	**94.3**	**94.3**

Table 6
Specificity(%) ±std of five models on 13 patients in the CHB-MIT dataset.

Patient ID	CNN	RDANet	Ours		
			CANet	RCANet	CRCANet
Pt01	98.9 ± 0.5	97.6 ± 0.8	99.1 ± 0.6	98.9 ± 0.8	**99.5 ± 0.3**
Pt02	91.0 ± 1.1	90.7 ± 1.1	90.0 ± 2.3	**92.2 ± 1.2**	91.5 ± 1.0
Pt03	98.4 ± 0.5	99.0 ± 0.5	99.4 ± 0.2	98.8 ± 0.5	**99.5 ± 0.3**
Pt05	86.3 ± 3.4	87.6 ± 1.6	**89.2 ± 2.5**	88.5 ± 1.6	88.4 ± 1.4
Pt09	99.8 ± 0.2	99.7 ± 0.4	**99.9 ± 0.2**	**99.9 ± 0.1**	**99.9 ± 0.2**
Pt10	94.9 ± 1.0	94.9 ± 0.6	95.0 ± 0.4	94.7 ± 1.5	**95.7 ± 1.0**
Pt13	94.6 ± 1.6	94.2 ± 2.0	95.5 ± 2.3	**96.5 ± 1.1**	96.1 ± 1.5
Pt14	73.5 ± 3.1	67.6 ± 1.7	71.4 ± 2.9	72.3 ± 1.1	**74.8 ± 1.8**
Pt18	**95.3 ± 0.8**	92.8 ± 1.0	94.4 ± 0.8	94.0 ± 1.6	94.7 ± 0.9
Pt19	99.0 ± 0.5	**99.4 ± 0.3**	99.1 ± 0.7	99.1 ± 0.2	99.2 ± 0.5
Pt20	99.7 ± 0.2	99.5 ± 0.3	**99.8 ± 0.2**	**99.8 ± 0.1**	**99.8 ± 0.2**
Pt21	74.7 ± 1.0	71.6 ± 2.3	75.6 ± 1.8	76.5 ± 1.6	**76.6 ± 2.0**
Pt23	99.3 ± 0.4	**99.6 ± 0.3**	99.2 ± 0.3	99.3 ± 0.1	99.5 ± 0.2
Average	92.7	91.9	92.9	93.1	**93.5**

EEG channels, while the recurrent criss-cross attention module enhances the representational capacity of the feature maps. By combining these two modules, further improvement is observed in the experimental results, indicating that CRCANet can effectively accomplish the task of seizure prediction.

To comprehensively analyze the epileptic seizure prediction performance of CRCANet, we compared its average results on the CHB-MIT dataset with those of CNN, ResNet, and RDANet. The comparison is shown in Fig. 9.

Compared to CNN, CRCANet shows improvements of 0.9 %, 0.8 %, and 0.8 % in average accuracy, sensitivity, and specificity, respectively. When compared to ResNet, CRCANet demonstrates improvements of 1.6 %, 1.5 %, and 1.7 % in those same metrics. And in comparison to RDANet, CRCANet's performance is better by 1.4 %, 1.0 %, and 1.6 % in average accuracy, sensitivity, and specificity, respectively. Evidently, CRCANet exhibits superior classification performance compared to other models. Additionally, the overall performance of RDANet is not outstanding. The primary reason lies in its construction based on ResNet, which requires extensive parameter training. However, the sample size of the CHB-MIT dataset is insufficient to adequately train a deep-level ResNet network, thereby affecting its classification performance. In contrast, CRCANet is better able to establish correlations between EEG channels while enhancing the pixel-level representation capability of feature maps. Due to its lightweight underlying network and other characteristics, it is more suitable for model training on the dataset used in this experiment.

To demonstrate the performance improvement of the model with different attention operations as a whole, we calculate the average accuracy, sensitivity, and specificity of experiments on 13 patients using four models, as shown in Fig. 10. The accuracy and sensitivity of CANet were both 0.4 % higher than those of CNN, while the specificity was 0.2 % higher. RCANet outperformed CNN with improvements of 0.6 % in accuracy, 0.8 % in sensitivity, and 0.4 % in specificity. This indicates that both the channel attention module and the recurrent criss-cross attention module effectively enhance the representation capacity of the feature maps. The CRCANet achieved a 0.9 % increase in accuracy, as well as enhancements of 0.8 % in sensitivity and specificity. The results above indicate that the combination of these two modules resulted in a further improvement in model performance, demonstrating the effectiveness of the fusion.

3.3. Analysis of model stability

To better evaluate the performance differences among the five models, this study randomly selected 8 patients and represented visually the results of each experimental group using box plots. One of the primary advantages of using box plots is their ability to accurately and consistently depict the discrete distribution of data. As shown in the Fig. 11, CRCANet exhibited the best stability and the highest accuracy on patients Chb01, Chb02, Chb03 and Chb13. However, CRCANet showed slightly less stability than the best performing model on patients Chb05, Chb14, Chb18 and Chb20, but still achieved the highest classification accuracy. In addition, CANet exhibited better stability on patients Chb14 and Chb20, while RCANet showed better stability on patients Chb05, Chb18 and Chb20. The above results indicate that CRCANet maintains the stability of the model while improving the classification accuracy. This suggests that channel attention module and recurrent criss-cross attention module have a positive effect on the stability of CRCANet. By introducing these two modules into the basic network, the classification performance of the model is optimized, and the reliability of the model in practical applications is also ensured.

3.4. Analysis of model efficiency

To evaluate the operational efficiency of the proposed model, we tested the training time of CRCANet per epoch on the data of each patient to quantify its computational complexity and operational efficiency. Meanwhile, we conducted comparative tests on three common epileptic seizure prediction models under the same experimental environment and configurations. Table 7 summarizes the average accuracy, sensitivity, specificity, training time per epoch and the size of training parameters for the four models.

It can be seen from the table that, compared with CNN, CRCANet has increased the average accuracy, sensitivity, and specificity by 0.9 %, 0.8 %, and 0.8 % respectively under the same training parameters, while the average training time has been reduced by 0.3 s; compared with ResNet, CRCANet has increased the average accuracy, sensitivity, and specificity by 1.6 %, 1.5 %, and 1.7 % respectively, with a significant reduction in the number of training parameters, and the average training time has been reduced by 2.3 s; compared with RDANet, CRCANet has increased the average accuracy, sensitivity, and specificity by 1.4 %, 1.0 %, and

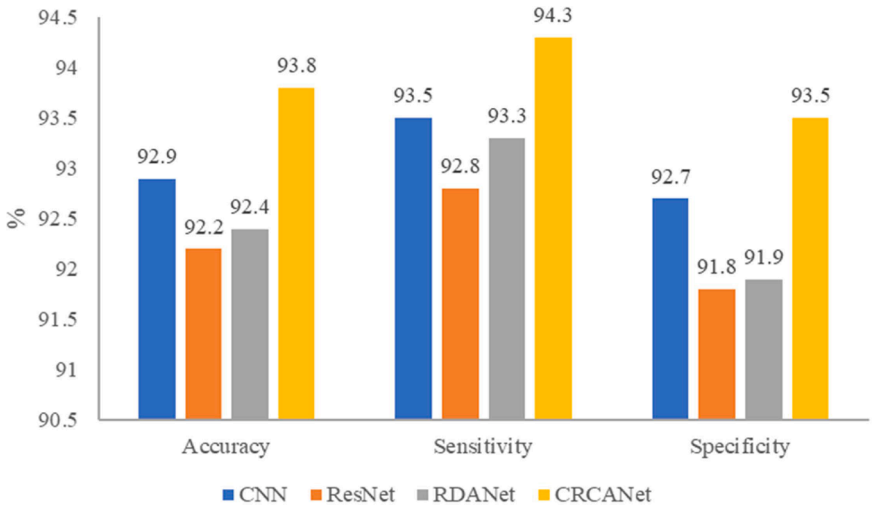

Fig. 9. The overall seizure prediction performance of CNN, ResNet, RDANet, CRCANet (When the horizontal axis is accuracy, sensitivity and specificity, respectively, the vertical axis also represents them).

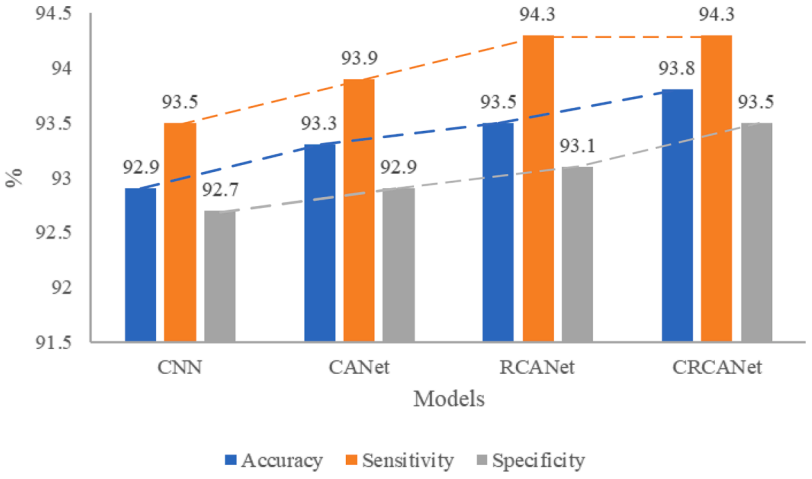

Fig. 10. The overall improvement of CNN by CANet, RCANet and CRCANet (When the bar chart is blue, orange, and gray, the vertical axis indicates accuracy, sensitivity, and specificity, respectively).

1.6 % respectively, with a significant reduction in the number of training parameters, and the average training time has been reduced by 1.9 s. The above comparison results show that CRCANet not only has a higher epileptic seizure prediction effect, but also has better operational efficiency.

4. Discussion

A variety of techniques have been developed to analyze EEG signals, including Fourier Transform (FT), Short-Time Fourier Transform (STFT), and Wavelet Transform (WT), which are widely applied in interpreting brain signals and detecting anomalies [42,43]. However, according to the study by Yang et al. [28], among various techniques, the processing performance of STFT in CHB-MIT was the best, helping the prediction model achieve the highest predictive performance. Therefore, we converted the original EEG signals into spectrograms by STFT in this study, while the vertical axis of the spectrogram represents time, and the horizontal axis represents frequency.

A criss-cross attention module can transfer the information contained in the pixels along the criss-cross paths in the spectrum feature map to the central pixel, so that the central pixel can obtain information from the pixels at its same time and frequency. When two criss-cross attention modules are stacked, the central pixel can acquire information from the entire feature map. CNN and recurrent criss-cross attention module form RCANet. After the RCANet operation, the information contained in the original point of the pixel occupies most weight, and other pixels with the same time and frequency occupy the second most weight, while pixels with different frequency and time occupy the least weight. Epileptic EEG datasets all have >20 channels [30,44-47]. And EEG channels often contain important information. However, RCANet does not pay attention to the interdependence between EEG channels, so we added a channel attention module to it to correlate channels and form CRCANet. In this way, we can obtain a feature map that contains both location and channel characteristics, further enhancing the representation ability of the feature map.

Table 8 shows some recent advances in epilepsy prediction research on the CHB-MIT dataset. Truong et al. [14] input the spectrograms into the three layers CNN and tested their approach with 13 patients identical to ours. Usman et al. [48] utilized a three-layer CNN for feature extraction and SVM for classification, while in another study [50], they employed LSTM for feature extraction on the spectrograms, achieving 93.0 % accuracy and 92.5 % sensitivity. Gao et al. [51] utilized Dilated CNN for feature extraction on the original EEG, obtaining 93.3 % sensitivity. Obviously, our model outperforms theirs in classification prediction performance.

Yang et al. [28] extracted spectrum and channel attention from the

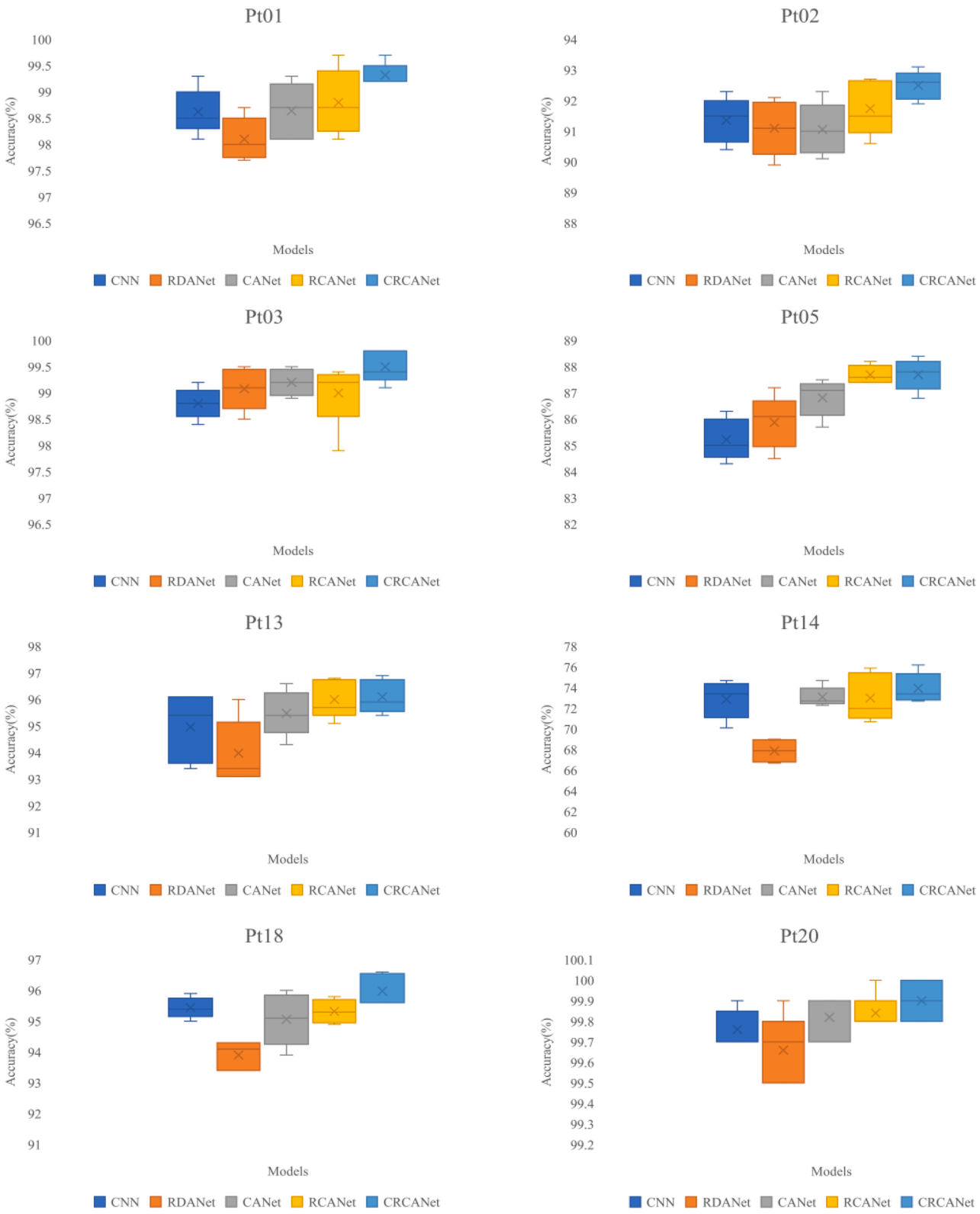

Fig. 11. Box plot of seizure prediction accuracy with five-fold cross validation in the CHB-MIT dataset of 8 patients.

feature map of the output of the deep convolutional model ResNet. Li et al. [49] utilized graph convolution (GCN) for epilepsy prediction. Zhang et al. [52] input the spectograms into Vision Transformer (ViT) to complete the task of feature extraction and classification. Training these models requires a significant amount of computational resources, resulting in low training efficiency. In comparison, this paper employs a lightweight CNN as the basic network, and the proposed CRCANet not only ensures prediction performance but also conserves computational resources.

Table 7
The average accuracy, sensitivity, specificity, training time per epoch and the size of training parameters of different methods on CHB-MIT.

Method	Acc(%)	Sens(%)	Spec(%)	Time(s)	Parameter(KB)
CNN	92.9	93.5	92.7	6.0	8442
ResNet	92.2	92.8	91.8	8.0	66,330
RDANet	92.4	93.3	91.9	7.6	66,330
CRCANet	93.8	94.3	93.5	5.7	8442

Table 8
Epilepsy prediction studies conducted on the CHB-MIT dataset in recent years.

Method	Accuracy (%)	Sensitivity (%)	Specificity (%)	Time (s)
EEG Spectrograms+CNN [14]	–	81.2	–	5.4
EEG Spectrograms+CNN+SVM [48]	–	92.7	90.8	–
EEG Spectrograms+RDANet [28]	92.07	89.25	92.67	7.6
Spatio-Temporal-Spectral features+GCN [49]	–	95.5	–	34.4
EEG Spectrograms+LSTM [50]	93.0	92.5	–	–
Raw EEG+Dilated CNN [51]	–	93.3	–	–
EEG Spectrograms+ViT [52]	81.2	75.6	81.8	8.2
STFT+CRCANet	**93.8**	**94.3**	**93.5**	**5.7**

5. Conclusion

In this study, we proposed the Channel Recurrent Criss-cross Attention Network (CRCANet) to predict the onset of epilepsy. It establishes connections between epileptic EEG channels through the channel attention module, while enhancing the information content of each pixel in the feature map through the recurrent criss-cross attention module, greatly enhancing the representation capability of the feature map. The experimental results show that CRCANet can efficiently complete the epileptic classification and prediction tasks. The patients in the CHB-MIT dataset are basically children, and in order to determine the overall performance of our model, our approach will be comprehensively tested in more different age groups in the future. And for achieving a better classification effect, we will study replacing CNN with a better model and still work on the attention mechanism in the future.

Ethical approval

Not required.

Declaration of competing interest

The authors declare that they have no known competing financial interests or personal relationships that could have appeared to influence the work reported in this paper.

Funding

This work was supported by the Key Research and Development Project of Zhejiang Province [grant number 2020C04009]; and Laboratory of Brain Machine Collaborative Intelligence of Zhejiang Province [grant number 2020E10010].

References

[1] Zheng Y, Jiang Z, Ping A, et al. Acute seizure control efficacy of multi-site closed-loop stimulation in a temporal lobe seizure model. IEEE Transac Neural Syst Rehabil Eng 2019;27(3):419–28.
[2] Kotsopoulos IAW, Van Merode T, Kessels FGH, et al. Systematic review and meta-analysis of incidence studies of epilepsy and unprovoked seizures. Epilepsia 2002;43(11):1402–9.
[3] Mahmoodian N, Boese A, Friebe M, et al. Epileptic seizure detection using cross-bispectrum of electroencephalogram signal. Seizure 2019;66:4–11.
[4] Zhan Q, Hu W. An epilepsy detection method using multiview clustering algorithm and deep features. Comput Math Methods Med 2020:2020.
[5] Shoeb AH, Guttag JV. Application of machine learning to epileptic seizure detection. In: Proceedings of the 27th international conference on machine learning (ICML-10); 2010. p. 975–82.
[6] Casson AJ, Yates DC, Smith SJM, et al. Wearable electroencephalography. IEEE Eng Med Biol Magazine 2010;29(3):44–56.
[7] Fisher RS, Cross JH, French JA, et al. Operational classification of seizure types by the international league against epilepsy: position paper of the ILAE commission for classification and terminology. Epilepsia 2017;58(4):522–30.
[8] Bhattacharya A, Baweja T, Karri SPK. Epileptic seizure prediction using deep transformer model. Int J Neural Syst 2022;32(02):2150058.
[9] Xu Y, Yang J, Sawan M. Multichannel synthetic preictal eeg signals to enhance the prediction of epileptic seizures. IEEE Transac Biomed Eng 2022;69(11):3516–25.
[10] Rajna P, Clemens B, Csibri E, et al. Hungarian multicentre epidemiologic study of the warning and initial symptoms (prodrome, aura) of epileptic seizures. Seizure 1997;6(5):361–8.
[11] Wei X, Zhou L, Zhang Z, et al. Early prediction of epileptic seizures using a long-term recurrent convolutional network. J Neurosci Methods 2019;327:108395.
[12] Ocak H. Automatic detection of epileptic seizures in EEG using discrete wavelet transform and approximate entropy. Expert Syst Appl 2009;36(2):2027–36.
[13] Islam MK, Rastegarnia A, Yang Z. A wavelet-based artifact reduction from scalp EEG for epileptic seizure detection. IEEE J Biomed Health Inform 2015;20(5):1321–32.
[14] Truong ND, Nguyen AD, Kuhlmann L, et al. Convolutional neural networks for seizure prediction using intracranial and scalp electroencephalogram. Neural Networks 2018;105:104–11.
[15] Park Y, Luo L, Parhi KK, et al. Seizure prediction with spectral power of EEG using cost-sensitive support vector machines. Epilepsia 2011;52(10):1761–70.
[16] Birjandtalab J, Jarmale VN, Nourani M, et al. Impact of personalization on epileptic seizure prediction. In: 2019 IEEE EMBS International Conference on Biomedical & Health Informatics (BHI). IEEE; 2019. p. 1–4.
[17] Abbaszadeh B, Yagoub MCE. Optimum window size and overlap for robust probabilistic prediction of seizures with iEEG. In: 2019 IEEE Conference on Computational Intelligence in Bioinformatics and Computational Biology (CIBCB). IEEE; 2019. p. 1–5.
[18] Aarabi A, He B. Seizure prediction in patients with focal hippocampal epilepsy. Clin Neurophysiol 2017;128(7):1299–307.
[19] Cho D, Min B, Kim J, et al. EEG-based prediction of epileptic seizures using phase synchronization elicited from noise-assisted multivariate empirical mode decomposition. IEEE Transac Neural Syst Rehabil Eng 2016;25(8):1309–18.
[20] Rim B, Sung NJ, Min S, et al. Deep learning in physiological signal data: a survey. Sensors 2020;20(4):969.
[21] Daoud H, Bayoumi MA. Efficient epileptic seizure prediction based on deep learning. IEEE Trans Biomed Circuits Syst 2019;13(5):804–13.
[22] Abdelhameed AM, Bayoumi M. An efficient deep learning system for epileptic seizure prediction. In: 2021 IEEE International Symposium on Circuits and Systems (ISCAS). IEEE; 2021. p. 1–5.
[23] Zhang S, Chen D, Ranjan R, et al. A lightweight solution to epileptic seizure prediction based on EEG synchronization measurement. J Supercomput 2021;77:3914–32.
[24] Hu W, Cao J, Lai X, et al. Mean amplitude spectrum based epileptic state classification for seizure prediction using convolutional neural networks. J Ambient Intell Humaniz Comput 2019:1–11.
[25] Cao J, Zhu J, Hu W, et al. Epileptic signal classification with deep EEG features by stacked CNNs. IEEE Transac Cognit Develop Syst 2019;12(4):709–22.
[26] Usman SM, Khalid S, Bashir S. A deep learning based ensemble learning method for epileptic seizure prediction. Comput Biol Med 2021;136:104710.
[27] Liu T, Truong ND, Nikpour A, et al. Epileptic seizure classification with symmetric and hybrid bilinear models. IEEE J Biomed Health Inform 2020;24(10):2844–51.
[28] Yang X, Zhao J, Sun Q, et al. An effective dual self-attention residual network for seizure prediction. IEEE Transac Neural Syst Rehabil Eng 2021;29:1604–13.
[29] Shoeb AH. Application of machine learning to epileptic seizure onset detection and treatment. Massachusetts Institute of Technology; 2009.
[30] Goldberger A, Amaral L, Glass L, et al. PhysioBank, PhysioToolkit, and PhysioNet: components of a new research resource for complex physiologic signals. Circulation 2000;101(23):e215–20.
[31] Klem GH. The ten-twenty electrode system of the international federation. the international federation of clinical neurophysiology. Electroencephalogr Clin Neurophysiol Suppl 1999;52:3–6.
[32] Litt B, Esteller R, Echauz J, et al. Epileptic seizures may begin hours in advance of clinical onset: a report of five patients. Neuron 2001;30(1):51–64.
[33] Fisher RS, Schachter SC. The postictal state: a neglected entity in the management of epilepsy. Epilepsy Behav. 2000;1(1):52–9.
[34] Maiwald T, Winterhalder M, Aschenbrenner-Scheibe R, et al. Comparison of three nonlinear seizure prediction methods by means of the seizure prediction characteristic. Physica D 2004;194(3–4):357–68.
[35] Truong ND, Kuhlmann L, Bonyadi MR, et al. Epileptic seizure forecasting with generative adversarial networks. IEEE Access 2019;7:143999–4009.
[36] Guo X, Yin Y, Dong C, et al. In: On the class imbalance problem//2008 Fourth international conference on natural computation. 4. IEEE; 2008. p. 192–201.
[37] Tsiouris KM, Pezoulas VC, Zervakis M, et al. A long short-term memory deep learning network for the prediction of epileptic seizures using EEG signals. Comput Biol Med 2018;99:24–37.

[38] Asif U, Roy S, Tang J, et al. SeizureNet: multi-spectral deep feature learning for seizure type classification. In: Machine Learning in Clinical Neuroimaging and Radiogenomics in Neuro-oncology: Third International Workshop, MLCN 2020, and Second International Workshop, RNO-AI 2020, Held in Conjunction with MICCAI 2020. Springer International Publishing; 2020. p. 77–87. October 4–8, 2020, Proceedings 3.
[39] Sriraam N, Temel Y, Rao SV, et al. A convolutional neural network based framework for classification of seizure types. In: 2019 41st Annual International Conference of the IEEE Engineering in Medicine and Biology Society (EMBC). IEEE; 2019. p. 2547–50.
[40] Fu J, Liu J, Tian H, et al. Dual attention network for scene segmentation. In: Proceedings of the IEEE/CVF conference on computer vision and pattern recognition; 2019. p. 3146–54.
[41] Huang Z, Wang X, Huang L, et al. Ccnet: criss-cross attention for semantic segmentation. In: Proceedings of the IEEE/CVF international conference on computer vision; 2019. p. 603–12.
[42] Samiee K, Kovacs P, Gabbouj M. Epileptic seizure classification of EEG time-series using rational discrete short-time Fourier transform. IEEE transac Biomed Eng 2014;62(2):541–52.
[43] Garg S, Narvey R. Denoising & feature extraction of EEG signal using wavelet transform. Int J Eng Sci Technol 2013;5(6):1249.
[44] Ihle M, Feldwisch-Drentrup H, Teixeira CA, et al. EPILEPSIAE–a European epilepsy database. Comput Methods Programs Biomed 2012;106(3):127–38.
[45] Andrzejak RG, Lehnertz K, Mormann F, et al. Indications of nonlinear deterministic and finite-dimensional structures in time series of brain electrical activity: dependence on recording region and brain state. Phys Rev E 2001;64(6):061907.
[46] Bbrinkm, Cukierski W. American epilepsy society seizure prediction challenge. kaggle, 2014, https://kaggle.com/competitions/seizure-prediction.
[47] Andrzejak RG, Schindler K, Rummel C. Nonrandomness, nonlinear dependence, and nonstationarity of electroencephalographic recordings from epilepsy patients. Phys Rev E 2012;86(4):046206.
[48] Usman SM, Khalid S, Aslam MH. Epileptic seizures prediction using deep learning techniques. IEEE Access 2020;8:39998–40007.
[49] Li Y, Liu Y, Guo YZ, et al. Spatio-temporal-spectral hierarchical graph convolutional network with semisupervised active learning for patient-specific seizure prediction. IEEE Trans Cybern 2021;52(11):12189–204.
[50] Usman SM, Khalid S, Bashir Z. Epileptic seizure prediction using scalp electroencephalogram signals. Biocybernet Biomed Eng 2021;41(1):211–20.
[51] Gao Y, Chen X, Liu A, et al. Pediatric seizure prediction in scalp EEG using a multi-scale neural network with dilated convolutions. IEEE J Transl Eng Health Med 2022;10:1–9.
[52] Zhang X, Li H. Patient-specific seizure prediction from scalp EEG using vision transformer. In: 2022 IEEE 6th Information Technology and Mechatronics Engineering Conference (ITOEC). 6. IEEE; 2022. p. 1663–7.